

# Lorentz Skew Scattering Mechanism in Nonreciprocal Magneto-Transport

Cong Xiao,<sup>1,\*</sup> Yue-Xin Huang,<sup>2,3,†</sup> and Shengyuan A. Yang<sup>1</sup>

<sup>1</sup>*Institute of Applied Physics and Materials Engineering, FST, University of Macau, Taipa, Macau SAR, China*

<sup>2</sup>*School of Sciences, Great Bay University, Dongguan 523000, China*

<sup>3</sup>*Great Bay Institute for Advanced Study, Dongguan 523000, China*

We unveil a new mechanism of nonreciprocal magneto-transport from cooperative action of Lorentz force and skew scattering. The significance of this Lorentz skew scattering mechanism lies in that it dominates both longitudinal and transverse responses in highly conductive systems, and it exhibits a scaling behavior distinct from all known mechanisms. At low temperature, it shows a cubic scaling in linear conductivity, whereas the scaling becomes quartic at elevated temperature when phonon scattering kicks in. We develop its microscopic formulation and reveal its close connection with Berry curvature on Fermi surface. Applying our theory to surface transport in topological crystalline insulator SnTe and bulk transport in Weyl semimetals leads to significant results, suggesting a new route to achieve giant transport nonreciprocity in high-mobility materials with topological band features.

Nonreciprocal transport phenomena have received significant attention, as they manifest intriguing physics of electronic quantum geometry and form the basis for rectification and diode applications [1–3]. Particularly, in nonmagnetic crystals with broken inversion symmetry, an applied magnetic field could trigger a nonreciprocal magneto-resistance linear in the  $B$  field [4–26]. The corresponding nonreciprocal magneto-transport (NRMT) response current can be expressed as  $j = \chi E^2 B$ , with  $\chi$  denoting the response tensor. This phenomenon was first studied in chiral crystals (known as electrical magnetochiral anisotropy) [1] and recently actively explored also in various achiral crystals [27–31].

In experiment, to understand microscopic mechanisms of a transport phenomenon, a common practice is to perform a scaling analysis, i.e., to analyze how the response coefficient varies as a function of the linear conductivity  $\sigma_{xx}$ , which is proportional to the scattering time  $\tau$ . Till now, several mechanisms for NRMT were proposed. For example, an intrinsic mechanism independent of  $\sigma_{xx}$  ( $\tau$ ) was revealed for NRMT Hall response [24, 32]. For longitudinal response,  $\chi$  may originate from chiral scatterer [1], magnetic self-field [1], Zeeman-coupling induced Fermi surface deformation [5, 33], energy relaxation [34], chiral anomaly [35] and Berry curvature [36] mechanisms in Weyl semimetals, and etc [37–39]. It is noted that: (1) theoretical formulations of the various mechanisms are so far limited within the simple relaxation time approximation which does not fully capture the quantum nature of scattering, and (2) they (except the intrinsic one) all give a  $\chi \propto \sigma_{xx}^2$  scaling. Thereby, a natural question arises: Is there any mechanism for NRMT, with distinct scaling behavior, from quantum effects in scattering? Furthermore, one may ask: What mechanism gives the *highest power* in the scaling relation? This is important, because such contribution is expected to dominate the response in clean samples with large  $\tau$ .

In this work, we answer the above questions by reveal-

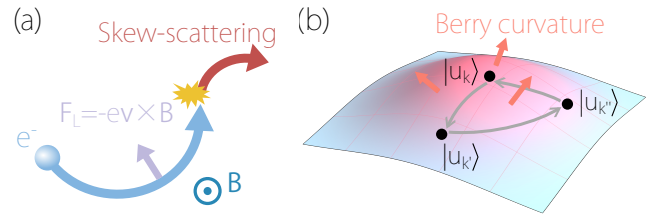


FIG. 1. (a) Schematic of actions of Lorentz force and skew scattering on electron motion. (b) Quantum geometric character of skew scattering process, as exemplified by a Wilson loop involving three states on Fermi surface. The corresponding skew scattering rate is proportional to the Berry curvature flux through the loop.

ing a new mechanism for NRMT — Lorentz skew scattering (LSK), which is resulted from the cooperative action of skew scattering (a quantum effect of scattering which induces trajectory skewness) and Lorentz force by magnetic field, as sketched in Fig. 1. This mechanism does not require spin-orbit coupling, and it manifests Berry curvature on Fermi surface. Importantly, we show that LSK is the leading contribution with the highest degree in the scaling relation for good metals. Specifically, at low temperatures when impurity scattering dominates, it gives  $\chi \propto \sigma_{xx}^3$  scaling; whereas at elevated temperatures when phonon scattering becomes substantial, the LSK contribution would scale as  $\sigma_{xx}^4$ . Because of its distinct scaling and quantum geometric character, it should be dominating in highly conductive samples and strongly enhanced by topological band features around Fermi level. We demonstrate our theory by studying surface transport in topological crystalline insulator SnTe and bulk transport in Weyl semimetals. The estimated LSK contribution can be orders of magnitude larger than previously studied mechanisms. As NRMT effect in most reported works is rather weak, our finding offers a new insight for amplifying this nonreciprocal effect, which is promising

for low-dissipative rectification applications.

*Geometric character and scaling behavior.* We consider a diffusive system under weak applied  $E$  and  $B$  fields in the semiclassical regime. The electric current is generally expressed as  $\mathbf{j} = -e \sum_l f_l \mathbf{v}_l$ , where  $-e$  is the electron charge,  $l = (n, \mathbf{k})$  is a collective index labeling a Bloch state,  $f$  is the distribution function, and  $v$  is the electron velocity. To study NRMT response, we focus only on the part of the current  $\propto E^2 B$ .

For our proposed LSK mechanism,  $B$  field enters via Lorentz force, while skew scattering enters via the collision integral. They together generate an out-of-equilibrium distribution  $f^{\text{LSK}} \propto E^2 B$ . (Hence, in calculating the current, it is sufficient to take  $v_l$  as the unperturbed band velocity.) This  $f^{\text{LSK}}$  can be obtained from the Boltzmann kinetic equation:

$$(\hat{D}_E + \hat{D}_L) f_l = (\hat{I}_c + \hat{I}_{\text{sk}}) f_l, \quad (1)$$

where hat denotes linear operators,  $\hat{D}_E = -\frac{e}{\hbar} \mathbf{E} \cdot \partial_{\mathbf{k}}$  and  $\hat{D}_L = -\frac{e}{\hbar} (\mathbf{v}_l \times \mathbf{B}) \cdot \partial_{\mathbf{k}}$  give the electric force and Lorentz force driving terms,  $\hat{I}_c$  and  $\hat{I}_{\text{sk}}$  correspond to the conventional collision integral  $\hat{I}_c f_l = -\sum_{l'} \omega_{l'l}^s (f_l - f_{l'})$  and the skew-scattering collision integral  $\hat{I}_{\text{sk}} f_l = -\sum_{l'} \omega_{l'l}^a (f_l + f_{l'})$ , respectively [40]. Here,  $\omega_{l'l}^s$  is the symmetric scattering rate between  $l$  and  $l'$  states, and  $\omega_{l'l}^a$  is the asymmetric (skew) scattering rate. For scaling analysis, one can take  $\hat{I}_c \sim 1/\tau$  and  $\hat{I}_{\text{sk}} \sim 1/\tau_{\text{sk}}$ , where the skew scattering time  $\tau_{\text{sk}}$  should be much larger than  $\tau$  [41, 42].

Assuming weak spin-independent disorders, the leading contribution to skew scattering is from third-order processes, with

$$\omega_{l'l}^a \approx \frac{4\pi^2}{\hbar} n_i \sum_{l''} \langle V_{ll''} V_{l''l'} V_{l'l} \rangle_c \delta(\varepsilon_{l'l}) \delta(\varepsilon_{l''l'}) \text{Im} W(l, l', l''), \quad (2)$$

where  $n_i$  is disorder density,  $V_{ll''} = V_{\mathbf{k}-\mathbf{k}'}$  is the Fourier component of disorder potential,  $\langle \dots \rangle_c$  denotes the disorder average,  $\varepsilon_{l'l} \equiv \varepsilon_{l'} - \varepsilon_l$ , and

$$W(l, l', l'') = \langle u_l | u_{l'} \rangle \langle u_{l'} | u_{l''} \rangle \langle u_{l''} | u_l \rangle \quad (3)$$

is a Wilson loop associated with the Pancharatnam-Berry phase  $\arg(W)$  [43]. For an infinitesimal Wilson loop in  $k$  space, one finds

$$\text{Im} W(l, l', l'') \approx \frac{1}{2} (\mathbf{k}'' - \mathbf{k}') \times (\mathbf{k}' - \mathbf{k}) \cdot \boldsymbol{\Omega}_l, \quad (4)$$

which is proportional to the Berry curvature  $\boldsymbol{\Omega}$ . It follows that for an isotropic model with smooth disorder potential,  $\omega_{l'l}^a \propto \mathbf{k}' \cdot (\mathbf{k} \times \boldsymbol{\Omega}_l)$ , explicitly showing the skewness of scattering, i.e., an incident electron with momentum  $\mathbf{k}$  tends to be scattered to the transverse direction  $\mathbf{k} \times \boldsymbol{\Omega}_l$ . Since the Lorentz force also deflects electrons, their cooperative action should affect both longitudinal and transverse current flows. And since for transport, scattering events occur mainly around Fermi level,

one expects that skew scattering (and LSK mechanism) would be enhanced if there is substantial Berry curvature distribution on Fermi surface.

Before detailed analysis, one may argue the scaling behavior of  $f^{\text{LSK}}$  in an intuitive way. The  $\tau$  dependence of out-of-equilibrium distribution is associated with the driving field.  $E$  field conventionally give a  $\propto \tau$  dependence, but with skew scattering, it leads to an additional contribution  $\propto \tau^2/\tau_{\text{sk}}$ , which has a higher degree in  $\tau$  and is well known in the study of anomalous Hall effect [44]. For  $f \propto E^2 B$ , if each factor of  $E$  is associated with conventional scattering and gives a  $\tau$  factor, the resulting distribution would be  $\propto \tau^2$ . This just corresponds to the previously studied mechanisms. Note that in those cases,  $B$  field only enters via correction of band structure and cannot bring additional  $\tau$  factors, because by itself a  $B$  field cannot drive a nonequilibrium. This also applies if one lets each  $E$  associated with skew scattering, then the result would scale as  $(\tau^2/\tau_{\text{sk}})^2$ . In comparison, a much larger contribution arises if  $B$  enters via Lorentz force: Combined with a factor of  $E$ , they together bring a  $\tau^2$  factor, which just corresponds to the ordinary Hall conductivity  $\propto \tau^2$  [45]. Then, combined with one skew scattering for the remaining  $E$  factor, we have a result  $\propto \tau^4/\tau_{\text{sk}}$ , which is the LSK contribution we are looking for. This analysis clarifies why LSK can have a higher  $\tau$  ( $\sigma_{xx}$ ) scaling than other mechanisms.

*Formulation of LSK & Diagrammatic approach.* To derive the formula for LSK contribution from Eq. (1), we use the method of successive approximations [40, 46, 47]. We expand the distribution function as

$$f = f^0 + \sum_{i,j} \left[ f^{(i,j)} + f_B^{(i,j)} \right]. \quad (5)$$

Here,  $f^0$  is the equilibrium Fermi-Dirac distribution. In the off-equilibrium part, we explicitly separate out the components  $f_B$  which are linear in  $B$ , and to keep track of the degrees in  $E$  field and scattering, we use the notation  $Q^{(i,j)}$  to indicate a quantity  $\propto E^i V^{-j}$ . In this notation, we have  $\hat{I}_c = \hat{I}_c^{(0,-2)}$  and  $\hat{I}_{\text{sk}} = \hat{I}_{\text{sk}}^{(0,-3)}$ . Our target is to solve  $f^{\text{LSK}}$ : It corresponds to certain  $f_B^{(2,j)}$  in the expansion (5) that involves one Lorentz force action ( $\hat{D}_L \hat{D}_E$ ) and one skew scattering ( $\hat{I}_{\text{sk}} \hat{D}_E$ ).

Substituting (5) into (1) and collecting terms at each order of fields and scattering strength, we obtain a set of coupled linear equations. For example, for terms linear in  $E$  ( $i = 1$ ), we have

$$\hat{I}_c f^{(1,2)} = \hat{D}_E f^0, \quad \hat{I}_c f_B^{(1,4)} = \hat{D}_L f^{(1,2)}, \quad (6)$$

and the remaining equations share common forms of

$$\hat{I}_c f^{(1,j)} = -\hat{I}_{\text{sk}} f^{(1,j+1)} \quad (j < 2), \quad (7)$$

$$\hat{I}_c f_B^{(1,j)} = \hat{D}_L f^{(1,j-2)} - \hat{I}_{\text{sk}} f_B^{(1,j+1)} \quad (j < 4). \quad (8)$$

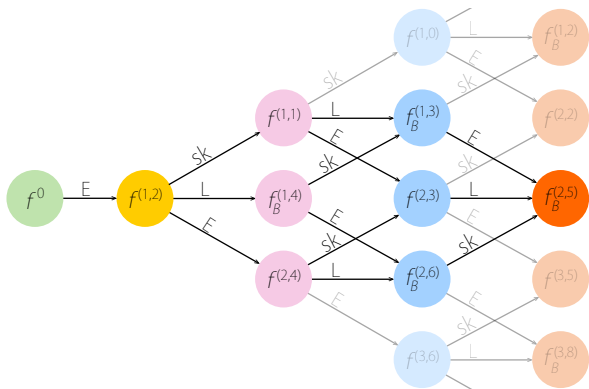


FIG. 2. Diagrammatic approach to solve the kinetic equation. Each node denotes a component  $f^{(i,j)}$ , and each arrow denotes an operation (rules are described in the text). Nodes in each column share the same dependence on  $\tau$ . From left to right, the components are  $\propto \tau^0, \tau^1, \tau^2, \tau^3$  and  $\tau^4$ , respectively. The components relevant to LSK are highlighted.

Similarly, one can write down the equations at  $E^2$  ( $i = 2$ ) order (presented in Supplemental Material [48]). These equations allow us to successively solve each  $f^{(i,j)}$ . For instance,  $f^{(1,2)} = \hat{\mathcal{I}}_c^{-1} \hat{\mathcal{D}}_E f^0 \sim \tau \hat{\mathcal{D}}_E f^0$  is the familiar

one responsible for Drude conductivity  $\sigma_{xx}$ ,  $f_B^{(1,4)} = \hat{\mathcal{I}}_c^{-1} \hat{\mathcal{D}}_L f^{(1,2)} \sim \tau^2 \hat{\mathcal{D}}_L \hat{\mathcal{D}}_E f^0$ , and so on.

We find that the construction of each  $f^{(i,j)}$  can be conveniently done in a diagrammatical way, as illustrated in Fig. 2. The *rules* are: (1) Each node is a component of distribution function, and the construction starts from  $f^0$ ; (2) An arrow with label  $O$  pointing from node  $A$  to  $B$  means  $f^B$  has a contribution from  $f^A$  acted by the operator  $\hat{O}$ , and the degrees of  $E, B, V$  must be balanced between  $f^B$  and  $\hat{O}f^A$ ; (3) Here, we have three types of arrow labels with the correspondence:  $E \rightarrow -\tau \hat{\mathcal{D}}_E$ ,  $L \rightarrow -\tau \hat{\mathcal{D}}_L$ , and  $sk \rightarrow \tau \hat{\mathcal{I}}_{sk}$ . (4) The component at a node is obtained by summing all contributions associated with arrows pointing to it. In addition, there is no arrow from  $f^0$  with  $L$  or  $sk$  label, since they cannot produce nonequilibrium distribution without  $E$ . Following these rules, one can readily obtain any desired component  $f^{(i,j)}$ .

Since  $f^{\text{LSK}}$  is the component that involves four operators:  $\hat{\mathcal{I}}_{sk}, \hat{\mathcal{D}}_L$ , and two  $\hat{\mathcal{D}}_E$ 's, one can easily identify it as  $f_B^{(2,5)}$  in Fig. 2. Its expression can also be readily read off from the diagram as

$$f^{\text{LSK}} = f_B^{(2,5)} = -\tau^4 \left[ \hat{\mathcal{D}}_E \{ \hat{\mathcal{D}}_L, \hat{\mathcal{I}}_{sk} \} + \hat{\mathcal{D}}_L \{ \hat{\mathcal{I}}_{sk}, \hat{\mathcal{D}}_E \} + \hat{\mathcal{I}}_{sk} \{ \hat{\mathcal{D}}_E, \hat{\mathcal{D}}_L \} \right] \hat{\mathcal{D}}_E f^0. \quad (9)$$

Here,  $\{.,.\}$  is the anticommutator of two operators. Combined with the band velocity, it gives the LSK response current in NRMT:

$$\mathbf{j}^{\text{LSK}} = -e \sum_l f_l^{\text{LSK}} \mathbf{v}_l, \quad (10)$$

from which the response tensor  $\chi^{\text{LSK}}$  can be extracted ( $j_a^{\text{LSK}} = \chi_{abcd}^{\text{LSK}} E_b E_c B_d$ , where summation over repeated Cartesian indices is implied).

We have a few remarks. First, from Eq. (9), the scaling behavior  $f^{\text{LSK}}, \chi^{\text{LSK}} \propto \tau^4 / \tau_{sk}$  is consistent with our previous analysis. However, to discuss the scaling of  $\chi^{\text{LSK}}$  with  $\sigma_{xx}$ , we have to distinguish two regimes. In the low temperature regime where impurity scattering dominates,  $\sigma_{xx}$  is usually varied by fabricating samples with varying impurity density  $n_i$ . For example, in Refs. [49, 50], this is done by making metal films with different thicknesses such that the effective  $n_i$  from surface scattering is varied. Since both  $\tau$  and  $\tau_{sk}$  are  $\propto n_i$ , we expect for such cases,  $\chi^{\text{LSK}} \propto \sigma_{xx}^3$ . On the other hand, at elevated temperatures where phonon scattering is substantial,  $\tau$  (and  $\sigma_{xx}$ ) is usually varied by temperature, due to phonon scattering. Meanwhile, phonons do not contribute to skew scattering [49, 51, 52], so  $\tau_{sk}$  is still

from impurity scattering. Therefore, one should observe  $\chi^{\text{LSK}} \propto \sigma_{xx}^4$ . These scaling behaviors are distinct from all previous mechanisms for NRMT.

Second, the diagrammatic approach developed here offers a general method to tackle the Boltzmann equation for nonlinear transport. The various processes involved in a response can be easily identified and intuitively visualized. Via this approach, we also find contributions from higher-order LSK processes, which are much smaller than  $f^{\text{LSK}}$  by factors  $(\tau/\tau_{sk})^2$  and  $(\tau/\tau_{sk})^4$ , so they can generally be neglected.

Finally, in our analysis of Eq. (1), we have neglected effects such as side jump process [44], field modification of bands and velocities, and field correction to collision integrals [53]. These effects may contribute to NRMT, but they do not contribute to LSK response and their scaling degree is lower than  $\chi^{\text{LSK}}$ .

**LSK response in Dirac model.** We first apply our theory to the 2D Dirac model:

$$H = \tau w k_y + v_x k_x \sigma_y - \tau v_y k_y \sigma_x + \Delta \sigma_z, \quad (11)$$

where  $\tau = \pm$  labels two Dirac valleys connected by time reversal operation  $\mathcal{T}$ , and  $\sigma$ 's are Pauli matrices. This model describes the surface states of topological crys-

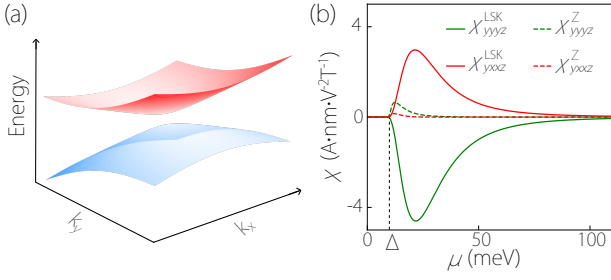


FIG. 3. (a) Dispersion of a 2D gapped Dirac valley in (11). (b) Calculated LSK nonlinear conductivities versus chemical potential for this model. For comparison, the dashed lines ( $\chi^Z$ 's) show the contribution from mechanism of Fermi surface deformation by Zeeman coupling to orbital moment. Here, we take parameters relevant to SnTe, with  $v_x/\hbar = v_y/\hbar = 4 \times 10^5$  m/s,  $\Delta = 10$  meV,  $w/v = 0.1$ ,  $n_i = 10^{10}$  cm $^{-2}$ , and averaged disorder strength  $V_0 = 10^{-13}$  eV  $\cdot$  cm $^2$ .

talline insulators SnTe [54] and Pb $_{1-x}$ Sn $_x$ Te(Se) [55] at low temperatures. The spectrum for one valley is shown in Fig. 3(a).

To have Lorentz force, we take  $B$  field to be in the  $z$  direction. Using Eqs. (9-10), near the bottom of the upper Dirac band, we estimate that the  $\chi^{\text{LSK}}$  components for both longitudinal and transverse NRMT can reach a similar order of magnitude, with (details in the Supplemental Material [48])

$$|\chi^{\text{LSK}}| \sim \frac{e^4 w}{\pi^2 \hbar^5 D} \frac{\tau^4}{\tau_{\text{sk}}}, \quad (12)$$

where  $D$  is the density of states. The results from numerical calculations (using parameters of SnTe [54, 56]) are plotted in Fig. 3(b), which exhibit a peak near band bottom, because of the sizable Berry curvature in this region. In the figure, for comparison, we also plot the results from the mechanism of Fermi surface deformation by Zeeman coupling to orbital moment ( $\chi^Z$ ) [33], which are found to be much smaller than the LSK mechanism.

The nonreciprocity is often characterized by the coefficient  $\eta = \delta\sigma/\sigma = -\delta\rho/\rho$ , measuring the change in conductivity (resistivity) when the current direction is reversed. Here, we find  $\eta$  from LSK can reach  $\sim 20\%$  under  $B = 1$  T and  $E = 10^4$  V/m. This value is orders of magnitude larger than several previous results of NRMT in 2D electron gas under similar field strengths [7, 8, 10]. Another figure of merit is the nonreciprocal coefficient  $\gamma = -\eta/IB$ , where  $I$  is the driving current [2]. For a sample width of 1  $\mu\text{m}$ , we estimate  $\gamma$  here can reach  $\sim 10^5$  A $^{-1}$ T $^{-1}$ , which is very large, considering that most reported  $\gamma$  values are below  $10^3$  A $^{-1}$ T $^{-1}$  [1, 4, 5, 7-10].

**Application to Weyl semimetal.** We have shown that to have pronounced LSK response, the system should have high mobility and large Berry curvature on Fermi surface. Weyl semimetals satisfy these conditions [57]. In a Weyl

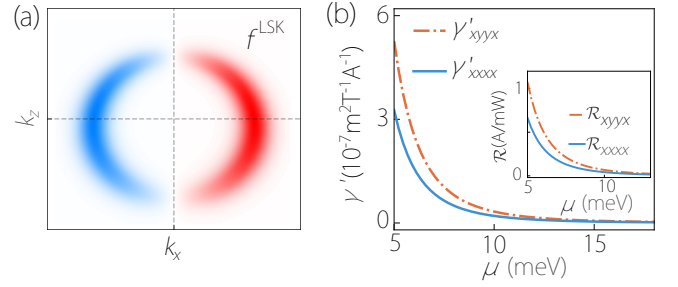


FIG. 4. LSK response for the Weyl model in Eq. (13). (a) Patterns of  $f^{\text{LSK}}$  on the Fermi surface in  $k_y = 0$  plane, for  $E$  and  $B$  fields applied in  $x$  direction and  $\mu = 10$  meV. (b) Calculated nonreciprocal coefficient  $\gamma'$  versus chemical potential. The inset shows the obtained current responsivity. In the calculation, we take  $B = 0.1$  T,  $v = 4 \times 10^5$  m/s,  $w/v = 0.4$ ,  $n_i = 10^{16}$  cm $^{-3}$ , and  $V_0 = 10^{-19}$  eV  $\cdot$  cm $^3$ .

semimetal, the low-energy physics is from states around Weyl points [57]. A generic model for a Weyl point can be written as

$$H = wk_z + vk \cdot \sigma, \quad (13)$$

which acts as a monopole for Berry curvature field. Since LSK contribution is  $\mathcal{T}$ -even, a pair of Weyl points connected by  $\mathcal{T}$  give the same contribution.

We perform numerical calculation for this Weyl model using parameters typical of Weyl semimetal materials (such as TaP family [58]). Figure 4(a) illustrates the obtained  $f^{\text{LSK}}$  distribution. For bulk materials, one usually characterizes NRMT using an intrinsic coefficient  $\gamma' = \gamma A = -\chi/\sigma_{xx}^2$ , where  $A$  is the cross sectional area of the sample [5, 27, 35]. Figure 4(b) shows the result. One finds that  $\gamma'$  can reach  $3 \times 10^{-7}$  m $^2$ A $^{-1}$ T $^{-1}$  for  $\mu = 5$  meV above Weyl point. Such LSK contribution is at least an order of magnitude larger than the chiral anomaly contribution and other mechanisms previously proposed [35]. This demonstrates LSK could dominate the NRMT response in Weyl semimetals.

**Discussion.** We have proposed a novel mechanism for NRMT. It is significant since it manifests quantum geometry of band structure (Berry curvature on Fermi surface) and is dominant in highly conductive samples. As we noted, materials with topological band features around Fermi level, such as topological semimetals, should be ideal systems to study this mechanism. Recently, signals of strong skew scattering effects in nonlinear Hall measurement were reported in several systems, such as twisted bilayer graphene [59, 60], BiTeBr [61] and Te thin flakes [62]. They could be promising platforms to explore LSK response as well.

The LSK mechanism is not limited to electrical transport but should also affect other processes, such as nonreciprocal thermal and thermoelectric transport. In particular, it may play an important role in thermal rectification [63, 64], which is an important direction of research.

The LSK induced NRMT is suitable for rectifier or detector applications, since such devices require high mobility materials, which could reduce power consumption and heat dissipation. An important metric for rectification applications is the current responsivity  $\mathcal{R} = j_{dc}/P$ , which is the ratio of the output dc current to the power dissipation  $P$  [65]. For the Weyl semimetal case, we estimate that  $\mathcal{R}$  due to LSK may reach  $\sim 0.66$  A/mW at  $\mu = 5$  meV, for  $B = 0.1$  T and a device size of  $1 \mu\text{m}$ , as shown in the inset of Fig. 4(b). This value is already orders of magnitude larger than other reported rectification mechanisms [65, 66]. All these suggest that rectification based on LSK indeed holds potential for practical applications.

\* xiaoziche@gmail.com; These authors contributed equally

† These authors contributed equally

- [1] G. L. J. A. Rikken, J. Fölling, and P. Wyder, *Phys. Rev. Lett.* **87**, 236602 (2001).
- [2] Y. Tokura and N. Nagaosa, *Nat. Commun.* **9**, 3740 (2018).
- [3] T. Ideue and Y. Iwasa, *Annu. Rev. Condens. Matter Phys.* **12**, 201 (2021).
- [4] F. Pop, P. Auban-Senzier, E. Canadell, G. L. Rikken, and N. Avarvari, *Nat. Commun.* **5**, 3757 (2014).
- [5] T. Ideue, K. Hamamoto, S. Koshikawa, M. Ezawa, S. Shimizu, Y. Kaneko, Y. Tokura, N. Nagaosa, and Y. Iwasa, *Nat. Phys.* **13**, 578 (2017).
- [6] S. S.-L. Zhang and G. Vignale, in *Spintronics XI*, Vol. 10732 (SPIE, 2018) pp. 97–107.
- [7] P. He, S. S.-L. Zhang, D. Zhu, Y. Liu, Y. Wang, J. Yu, G. Vignale, and H. Yang, *Nat. Phys.* **14**, 495 (2018).
- [8] P. He, S. M. Walker, S. S.-L. Zhang, F. Y. Bruno, M. S. Bahramy, J. M. Lee, R. Ramaswamy, K. Cai, O. Heinonen, G. Vignale, F. Baumberger, and H. Yang, *Phys. Rev. Lett.* **120**, 266802 (2018).
- [9] G. L. J. A. Rikken and N. Avarvari, *Phys. Rev. B* **99**, 245153 (2019).
- [10] D. Choe, M.-J. Jin, S.-I. Kim, H.-J. Choi, J. Jo, I. Oh, J. Park, H. Jin, H. C. Koo, B.-C. Min, *et al.*, *Nat. Commun.* **10**, 4510 (2019).
- [11] T. Guillet, C. Zucchetti, Q. Barbedienne, A. Marty, G. Isella, L. Cagnon, C. Vergnaud, H. Jaffrès, N. Reyren, J.-M. George, A. Fert, and M. Jamet, *Phys. Rev. Lett.* **124**, 027201 (2020).
- [12] A. Dyrdał, J. Barnaś, and A. Fert, *Phys. Rev. Lett.* **124**, 046802 (2020).
- [13] Y. Li, Y. Li, P. Li, B. Fang, X. Yang, Y. Wen, D.-x. Zheng, C.-h. Zhang, X. He, A. Manchon, *et al.*, *Nat. Commun.* **12**, 540 (2021).
- [14] F. Calavalle, M. Suárez-Rodríguez, B. Martín-García, A. Johansson, D. C. Vaz, H. Yang, I. V. Maznichenko, S. Ostanin, A. Mateo-Alonso, A. Chuvilin, *et al.*, *Nat. Mater.* **21**, 526 (2022).
- [15] H. F. Legg, M. Rößler, F. Munning, D. Fan, O. Breunig, A. Bliesener, G. Lippertz, A. Uday, A. Taskin, D. Loss, *et al.*, *Nat. Nanotechnol.* **17**, 696 (2022).
- [16] Y. Zhang, V. Kalappattil, C. Liu, M. Mehraeen, S. S.-L. Zhang, J. Ding, U. Erugu, Z. Chen, J. Tian, K. Liu, *et al.*, *Sci. Adv.* **8**, eabo0052 (2022).
- [17] Y. Wang, B. Liu, Y.-X. Huang, S. V. Mambakkam, Y. Wang, S. A. Yang, X.-L. Sheng, S. A. Law, and J. Q. Xiao, *Phys. Rev. B* **106**, L241401 (2022).
- [18] G. Tuvia, A. Burshtein, I. Silber, A. Aharony, O. Entin-Wohlman, M. Goldstein, and Y. Dagan, *Phys. Rev. Lett.* **132**, 146301 (2024).
- [19] P. He, S. S.-L. Zhang, D. Zhu, S. Shi, O. G. Heinonen, G. Vignale, and H. Yang, *Phys. Rev. Lett.* **123**, 016801 (2019).
- [20] P. He, C.-H. Hsu, S. Shi, K. Cai, J. Wang, Q. Wang, G. Eda, H. Lin, V. M. Pereira, and H. Yang, *Nat. Commun.* **10**, 1290 (2019).
- [21] W. Rao, Y.-L. Zhou, Y.-j. Wu, H.-J. Duan, M.-X. Deng, and R.-Q. Wang, *Phys. Rev. B* **103**, 155415 (2021).
- [22] Y. Kozuka, S. Isogami, K. Masuda, Y. Miura, S. Das, J. Fujioka, T. Ohkubo, and S. Kasai, *Phys. Rev. Lett.* **126**, 236801 (2021).
- [23] S. Gholizadeh, J. H. Cullen, and D. Culcer, *Phys. Rev. B* **107**, L041301 (2023).
- [24] Y.-X. Huang, X. Feng, H. Wang, C. Xiao, and S. A. Yang, *Phys. Rev. Lett.* **130**, 126303 (2023).
- [25] R. M. A. Dantas, H. F. Legg, S. Bosco, D. Loss, and J. Klinovaja, *Phys. Rev. B* **107**, L241202 (2023).
- [26] C. Niu, G. Qiu, Y. Wang, P. Tan, M. Wang, J. Jian, H. Wang, W. Wu, and P. D. Ye, *Nano letters* **23**, 8445 (2023).
- [27] Y. Wang, H. F. Legg, T. Bömerich, J. Park, S. Biesenkamp, A. A. Taskin, M. Braden, A. Rosch, and Y. Ando, *Phys. Rev. Lett.* **128**, 176602 (2022).
- [28] Y. Wang, T. Bömerich, J. Park, H. F. Legg, A. A. Taskin, A. Rosch, and Y. Ando, *Phys. Rev. Lett.* **131**, 146602 (2023).
- [29] N. Wang, J.-Y. You, A. Wang, X. Zhou, Z. Zhang, S. Lai, Y.-P. Feng, H. Lin, G. Chang, and W.-b. Gao, *Nat. Sci. Rev.* **11**, nwad103 (2024).
- [30] X. Zhang, T. Zhu, S. Zhang, Z. Chen, A. Song, C. Zhang, R. Gao, W. Niu, Y. Chen, F. Fei, *et al.*, *Nat. Commun.* **15**, 2992 (2024).
- [31] C. Li, R. Wang, S. Zhang, Y. Qin, Z. Ying, B. Wei, Z. Dai, F. Guo, W. Chen, R. Zhang, *et al.*, *Nat. Mater.* **1** (2024).
- [32] Y.-X. Huang, Y. Wang, H. Wang, C. Xiao, X. Li, and S. A. Yang, *Phys. Rev. B* **108**, 075155 (2023).
- [33] S. Okumura, R. Tanaka, and D. Hirobe, *Phys. Rev. B* **110**, L020407 (2024).
- [34] L. E. Golub, E. L. Ivchenko, and B. Spivak, *Phys. Rev. B* **108**, 245202 (2023).
- [35] T. Morimoto and N. Nagaosa, *Phys. Rev. Lett.* **117**, 146603 (2016).
- [36] T. Yokouchi, Y. Ikeda, T. Morimoto, and Y. Shiomi, *Phys. Rev. Lett.* **130**, 136301 (2023).
- [37] S. Lahiri, T. Bhore, K. Das, and A. Agarwal, *Phys. Rev. B* **105**, 045421 (2022).
- [38] J.-Y. Ba, Y.-M. Wang, H.-J. Duan, M.-X. Deng, and R.-Q. Wang, *Phys. Rev. B* **108**, L241104 (2023).
- [39] H. J. Zhao, L. Tao, Y. Fu, L. Bellaiche, and Y. Ma, *Phys. Rev. Lett.* **133**, 096802 (2024).
- [40] N. A. Sinitsyn, *J. Phys.: Condens. Matter* **20**, 023201 (2007).
- [41] N. A. Sinitsyn, J. E. Hill, H. Min, J. Sinova, and A. H. MacDonald, *Phys. Rev. Lett.* **97**, 106804 (2006).
- [42] P. He, H. Isobe, D. Zhu, C.-H. Hsu, L. Fu, and H. Yang,

- Nat. Commun.* **12**, 698 (2021).
- [43] D. Vanderbilt, *Berry Phases in Electronic Structure Theory: Electric Polarization, Orbital Magnetization and Topological Insulators* (Cambridge University Press, 2018).
- [44] N. Nagaosa, J. Sinova, S. Onoda, A. H. MacDonald, and N. P. Ong, *Rev. Mod. Phys.* **82**, 1539 (2010).
- [45] J. M. Ziman, *Principles of the Theory of Solids* (Cambridge, Londo, 1972).
- [46] C. Xiao, Z. Z. Du, and Q. Niu, *Phys. Rev. B* **100**, 165422 (2019).
- [47] Y.-X. Huang, C. Xiao, S. A. Yang, and X. Li, [arXiv:2311.01219](https://arxiv.org/abs/2311.01219).
- [48] See Supplemental Material for the Boltzmann equations at  $E^2$  order and details of the 2D Dirac model related to surface states of topological crystalline insulators.
- [49] D. Hou, G. Su, Y. Tian, X. Jin, S. A. Yang, and Q. Niu, *Phys. Rev. Lett.* **114**, 217203 (2015).
- [50] D. Yue and X. Jin, *J. Phys. Soc. Jpn.* **86**, 011006 (2017).
- [51] S.-K. Lyo, *Phys. Rev. B* **8**, 1185 (1973).
- [52] S. A. Yang, H. Pan, Y. Yao, and Q. Niu, *Phys. Rev. B* **83**, 125122 (2011).
- [53] C. Xiao, H. Chen, Y. Gao, D. Xiao, A. H. MacDonald, and Q. Niu, *Phys. Rev. B* **101**, 201410(R) (2020).
- [54] Y. Tanaka, Z. Ren, T. Sato, K. Nakayama, S. Souma, T. Takahashi, K. Segawa, and Y. Ando, *Nat. Phys.* **8**, 800 (2012).
- [55] Y. Okada, M. Serbyn, H. Lin, D. Walkup, W. Zhou, C. Dhital, M. Neupane, S. Xu, Y. J. Wang, R. Sankar, F. Chou, A. Bansil, M. Z. Hasan, S. D. Wilson, L. Fu, and V. Madhavan, *Science* **341**, 1496 (2013).
- [56] I. Sodemann and L. Fu, *Phys. Rev. Lett.* **115**, 216806 (2015).
- [57] N. P. Armitage, E. J. Mele, and A. Vishwanath, *Rev. Mod. Phys.* **90**, 015001 (2018).
- [58] D. Grassano, O. Pulci, E. Cannuccia, and F. Bechstedt, *Eur. Phys. J. B* **93**, 157 (2020).
- [59] P. He, G. K. W. Koon, H. Isobe, J. Y. Tan, J. Hu, A. H. C. Neto, L. Fu, and H. Yang, *Nat. Nanotechnol.* **17**, 378 (2022).
- [60] J. Duan, Y. Jian, Y. Gao, H. Peng, J. Zhong, Q. Feng, J. Mao, and Y. Yao, *Phys. Rev. Lett.* **129**, 186801 (2022).
- [61] X. F. Lu, C.-P. Zhang, N. Wang, D. Zhao, X. Zhou, W. Gao, X. H. Chen, K. Law, and K. P. Loh, *Nat. Commun.* **15**, 245 (2024).
- [62] B. Cheng, Y. Gao, Z. Zheng, S. Chen, Z. Liu, L. Zhang, Q. Zhu, H. Li, L. Li, and C. Zeng, *Nat. Commun.* **15**, 5513 (2024).
- [63] N. A. Roberts and D. Walker, *Int. J. Therm. Sci.* **50**, 648 (2011).
- [64] N. Li, J. Ren, L. Wang, G. Zhang, P. Hänggi, and B. Li, *Rev. Mod. Phys.* **84**, 1045 (2012).
- [65] Y. Zhang and L. Fu, *Proc. Natl. Acad. Sci. U.S.A.* **118**, 10.1073/pnas.2100736118 (2021).
- [66] A. Rogalski, M. Kopytko, and P. Martyniuk, *Applied Physics Reviews* **6**, 10.1063/1.5088578 (2019).